Supplementary Information for

Exciting Andreev pairs in a superconducting atomic contact

L. Bretheau, Ç. Ö. Girit, H. Pothier, D. Esteve and C. Urbina

1 Supplementary Figures and Legends

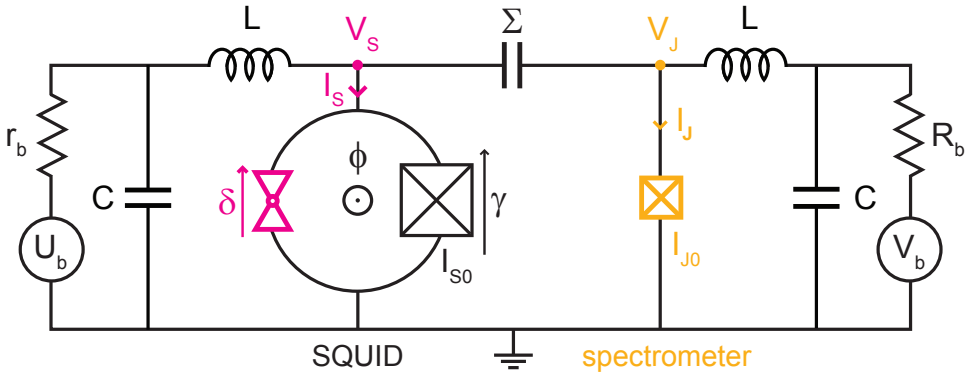

Supplementary Figure 1: Equivalent circuit for the experiment. The spectrometer [respectively the SQUID] is biased by a voltage source V_b [U_b] through an on-chip LC filter ($L \simeq 0.89\,\mathrm{nH}$, $C \simeq 20\,\mathrm{pF}$) and a series resistance $R_b = 2\mathrm{k}\Omega$ [$r_b = 200\Omega$] mounted at the same temperature as the sample. The current I_J [I_S] is measured from the voltage drop across R_b [r_b]. These two circuits are decoupled at dc, but strongly coupled at the frequencies relevant for the spectroscopy through the on-chip capacitor $\Sigma \simeq 30$ pF. At the high frequencies involved in the spectroscopy experiments, the capacitors C and Σ can be considered essentially as shorts. The spectrometer essentially probes the SQUID in parallel with an inductor $L/2 \simeq 445\,\mathrm{pH}$, which renormalizes the characteristic impedance and the frequency of its plasma mode.

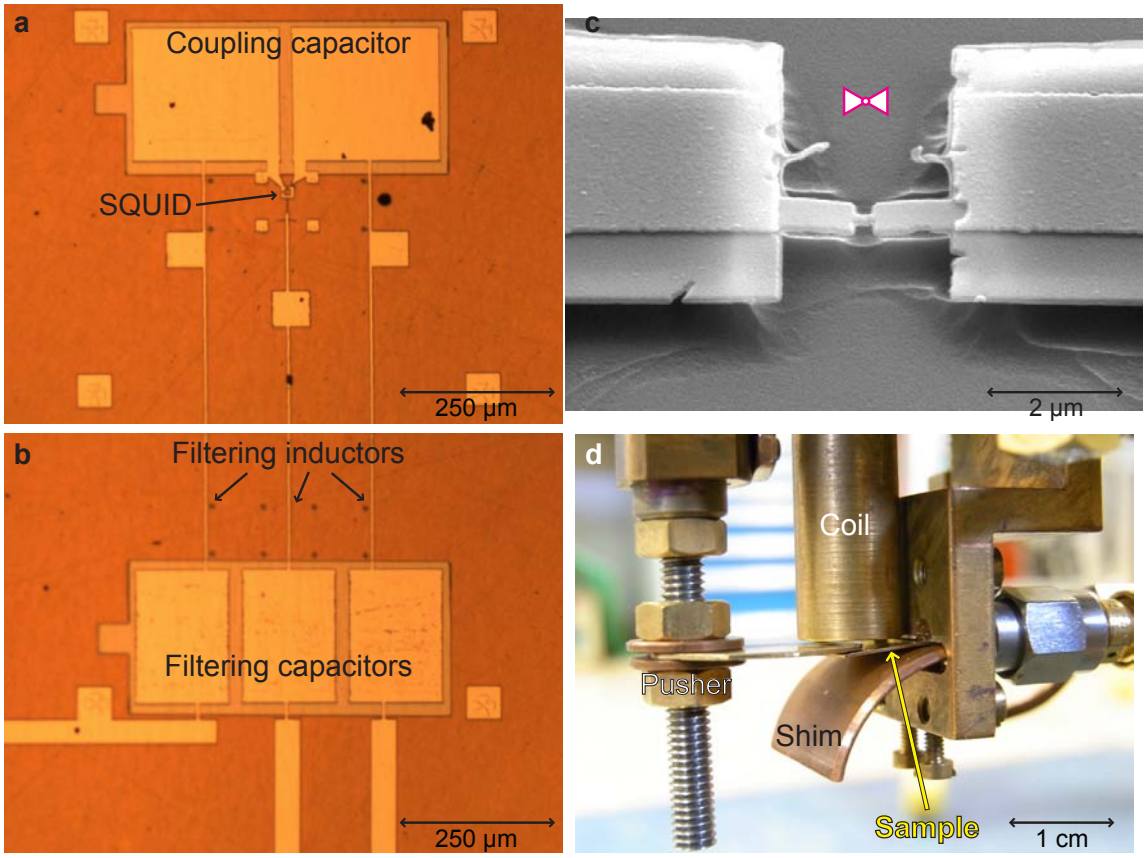

Supplementary Figure 2: Views of the sample. **a,** Optical micrograph of the capacitor coupling the SQUID to the spectrometer. It is formed by two Al electrodes $230 \times 220\,\mu m^2$ separated by a 55 nm thick alumina layer from a $500 \times 250\,\mu m^2$ Al bottom electrode. The three 5 µm-wide, 1.38 mm-long lines, form the inductors of the on-chip LC filters. **b,** Optical micrograph of the filtering capacitors: bottom electrode $350 \times 250\,\mu m^2$, top electrodes $146 \times 220\,\mu m^2$. **c,** Scanning electron micrograph of the suspended bridge forming the atomic contacts. Picture taken at an angle. **d,** Sample holder attached to the mixing chamber of a dilution refrigerator. The 14mm$\times$14mm sample is clamped to two SMA launchers connecting it to the biasing and measuring lines. The threaded spindle, actuated by a room temperature dc motor, controls the bending of the substrate. A curved shim below the flexible substrate forces an homogeneous bending. The copper cylinder above the sample houses a superconducting coil.

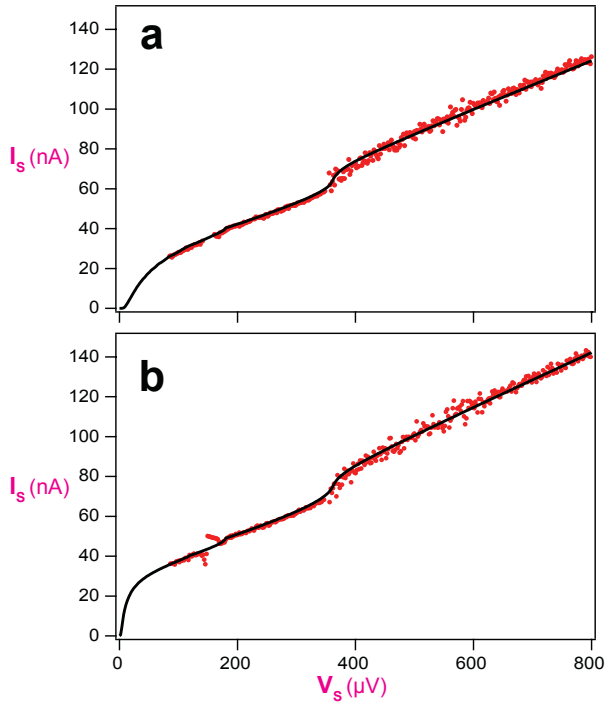

Supplementary Figure 3: IV characteristics of AC1 (a) and AC2 (b). They are obtained after subtracting the Josephson junction characteristic from that of the respective SQUIDs. Solid lines are fits with the theory of Multiple Andreev Reflections[?], excluding the region $|V| < 200$ μeV where the IV characteristic of the SQUID junction alone presents resonances, yielding the transmissions $\{0.942, 0.26, 0.08 \times 4\}$ for AC1 and $\{0.985, 0.37, 0.12 \times 4\}$ for contact AC2. Because the SQUID junction by itself displays significant subgap current due to resonances, the method is not as precise as for isolated atomic contacts. In practice, the weak transmissions are not determined to better than a few percent. This is why we take degenerate values for the weakest transmitted channels of both contacts.

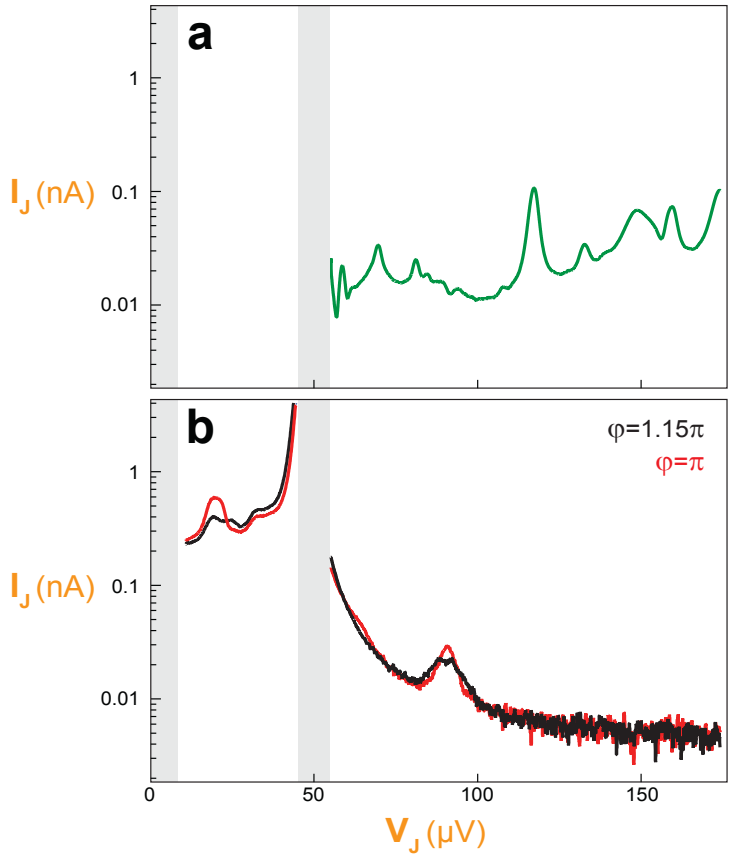

Supplementary Figure 4: Background current and IVs at different fluxes. **a,** Flux-independent background current of the spectrometer. **b,** Current-voltage $I_J(V_J)$ characteristics of the spectrometer for contact AC2, for fluxes $\varphi = 1.15\,\pi$ (black line) and $\varphi = \pi$ (red line), after subtraction of the flux-independent background.

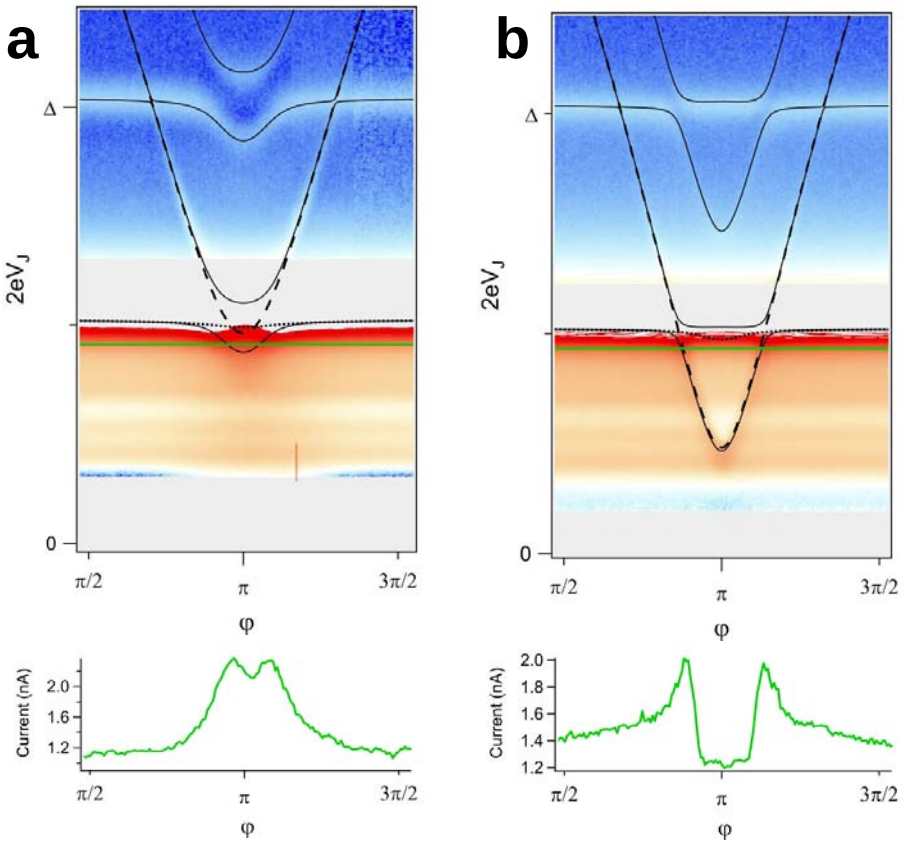

Supplementary Figure 5: Hybridization between plasma and Andreev levels. Experimental spectra of (**a**) AC1 and (**b**) AC2 (top panels) with green lines indicating position of line traces at constant voltage shown in bottom panels. The positions of the line traces are such that the theory without hybridization (dashed lines, bare Andreev transition; dotted lines, bare plasma transition) would predict a peak in absorption at $\varphi \approx \pi$ rather than a dip as observed in both experimental line traces. In the case of (**a**) AC1, a peak is expected as a result of summing the weights of the bare Andreev (dashed line) and bare plasma transitions (dotted line) at the level crossing, $\varphi \approx \pi$, $2eV_J = h\nu_p$. In the case of (**b**) AC2 the peak is expected as a result of the shift toward lower energy of the bare plasma transition at $\varphi \approx \pi$. The experimental line traces are consistent only with the full theory which predicts hybridization (black lines).

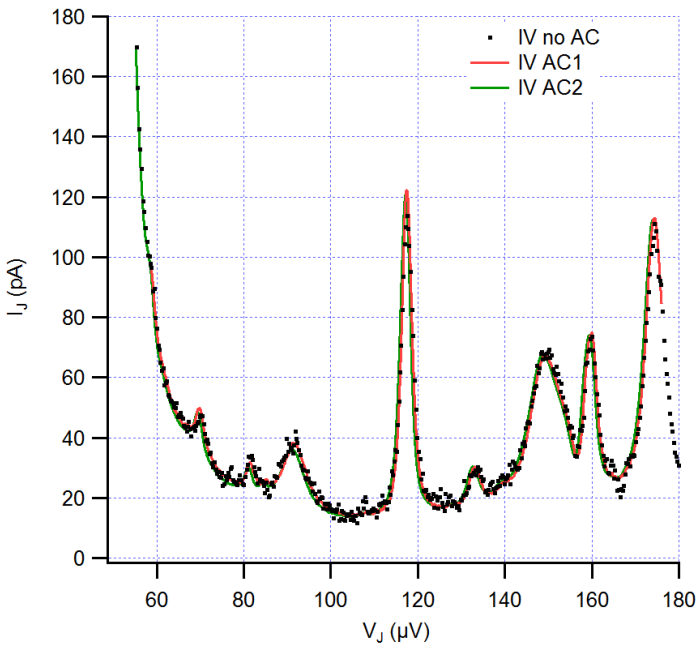

Supplementary Figure 6: Comparison of Spectrometer IVs with and without Atomic Contact. Current-voltage characteristics of the spectrometer for AC1 (red line), AC2 (green line), and with the break junction open (no atomic contact, black dots). The flux through the SQUID is $\varphi \approx 0$.

2 Supplementary Methods

2.1 Sample fabrication and measurement setup

The exact fabrication recipe can be found in Reference 31.

The sample was fabricated on a 300 µm-thick bronze plate covered with a 2-µm thick insulating polyimide layer. In a first e-beam lithography step, two 25 nm-thick Al electrodes are deposited to define the bottom electrodes of the coupling and filtering capacitors. The dielectric layer is formed by e-beam deposition of alumina performed at an angle and under planetary rotation of the sample in order to cover all the edges of the metallic electrodes. In a second

lithography step, all the rest of the circuit is drawn. A 50 nm-thick layer of Al is deposited and then oxidized to create the tunnel barriers of the Josephson junctions. Finally, 80 nm of Al are deposited under an angle of $53°$ to form both the SQUID and the spectrometer junctions at overlaps between the two layers. The SQUID and the spectrometer are connected to two electrodes which form the top electrodes of the coupling capacitor (Supplementary Figure 2a). Three narrow lines form the filtering inductors (~ 0.3 pH/μm according to simulations, using a dielectric constant 2.7 for polyimide[32]). These three lines end at three rectangular electrodes overlapping the second bottom electrode of the first step, defining the on-chip filtering capacitors (Supplementary Figure 2b). From there, much wider lines connect to large contact pads. In a last step, the polyimide underlayer is etched by reactive ion etching to suspend the bridge of the breakjunction (Supplementary Figure 2c).

The SQUID junction area is ~ 4.7 μm^2 and its critical current $I_{S0} = 1.06\,\mu$A (resistance $285\,\Omega$). The critical current of the spectrometer is $I_{J0} = 48\,$nA (resistance $6.3\,$kΩ). The total capacitance of the junctions $C_S \simeq 280\,$fF and the parallel inductor $L/2 \simeq 445\,$pH were found by fitting both the plasma frequency and the anti-crossing between the Andreev and plasma mode in contact $AC2$.

2.2 Background subtraction procedure

Figure 2 shows an example of raw IVs of the spectrometer. The sharp peaks above $50\,\mu$V which do not depend on the flux, are attributed to resonances in the environment of the spectrometer that do not involve the SQUID. They are subtracted from the measured spectra for AC1 and AC2 using the following procedure:

- The IV curves of the spectrometer for $V_J > 50\,\mu$V are averaged in a small interval around $\varphi = 0$. In this flux interval, as expected, no Andreev resonance is visible and the plasma

resonance does not change position significantly. When the kinetic inductance of the atomic contact is negligible with respect to that of the SQUID tunnel junction, as is the case for AC1 and AC2, the flux-averaged *IV* is identical to the IV taken when the break junction is open (see Supplementary Figure 6). This would not be the case for a more symmetric SQUID such as AC3.

- A fit of this curve is performed using a set of Lorentzian peaks. The two Lorentzians for the peaks at $V_J \simeq 45\,\mu\text{V}$ and $90\,\mu\text{V}$, which correspond respectively to the plasma resonance and to its first harmonic, are subtracted from the averaged $I_J\left(V_J\right)$, to obtain the background shown in the top panel of Supplementary Figure 4.

- This background is subtracted from each of the $I_J\left(V_J\right)$ curves taken at different φ. Supplementary Figure 4b shows the same IVs as in Figure 2 but with the background subtracted.

2.3 Spectrum calculation

To calculate the different transitions, we restrict the circuit probed by the spectrometer to the atomic-SQUID. Its Hamiltonian

$$H_{SQUID} = H_A(\delta) + h\nu_p^0(a^+a + \frac{1}{2})$$

contains two terms. The first one is the Andreev Hamiltonian[?] describing a single channel atomic contact:

$$H_A(\delta) = \Delta \exp\left(-i\sigma_x\sqrt{r}\delta/2\right)\left(\cos\left(\delta/2\right)\sigma_z + \sqrt{r}\sin\left(\delta/2\right)\sigma_y\right)$$

where the σ_i are the Pauli matrices and $r = 1 - \tau$ is the channel reflection probability. Its

eigenstates are the Andreev pair states $|-\rangle$ and $|+\rangle$, with eigenenergies $\mp E_A$. The physics of an Andreev pair is analogous to that of a spin-$1/2$ particle in a magnetic field whose amplitude E_A and direction depend both on the phase δ. The second term describes the Josephson junction of the SQUID, which is treated simply as an harmonic oscillator of frequency

$$\nu_p^0 = \frac{1}{2\pi\sqrt{L_S^0 C_S}},$$

the plasma frequency. The inductor L_S^0 is the Josephson inductor of the SQUID junction renormalized by the parallel inductor $L/2$: $L_S^0 = \left(2\pi I_{S0}/\phi_0 + 2/L\right)^{-1}$. The phase γ across the SQUID Josephson junction is related to the creation and annihilation operators by:

$$\gamma = \sqrt{z}\left(a + a^\dagger\right).$$

The dimensionless parameter z determines the amplitude of phase fluctuations

$$z = \pi Z_0 / R_Q$$

where $Z_0 = \sqrt{L_S^0/C_S}$ is the characteristic impedance of the oscillator.

Since δ and γ are linked by the flux φ, the two terms of the Hamiltonian are implicitly coupled and describe a spin-boson system[33,34]. The spectra presented in Figure 4C&E result from its numerical diagonalisation.

References

[31] Landry Bretheau, PhD thesis (2012), Localized excitations in superconducting point contacts: probing the Andreev doublet. Available on-line at http://tel.archives-ouvertes.fr.

[32] G. Ponchak and A. Downey, Characterization of thin film microstrip lines on polyimide. *IEEE Trans. Compon. Packag. Manuf. Technol.* **21**, 171 (1998).

[33] A. J. Leggett *et al.*, Dynamics of the dissipative two-state system, *Rev. Mod. Phys.* **59**, 1 (1987).

[34] U. Weiss, *Quantum Dissipative Systems* (World Scientific, Singapore, 1999).